# $^{99m}$Tc-Labeled Duramycin as a Novel Phosphatidylethanolamine-Binding Molecular Probe

Ming Zhao, Zhixin Li, and Scott Bugenhagen

*Department of Biophysics, Medical College of Wisconsin, Milwaukee, Wisconsin*

With only 19 amino acids, duramycin is the smallest known polypeptide that has a defined 3-dimensional binding structure. Duramycin binds phosphatidylethanolamine (PtdE) at a 1:1 ratio with high affinity and exclusive specificity. As an abundant binding target, PtdE is a major phospholipid and accounts for about 20% of the phospholipid content in mammalian cellular membranes. PtdE is externalized to the surface of apoptotic cells and also becomes accessible in necrotic cells because of compromised plasma membrane integrity. Given the unique physicochemical properties of duramycin and the availability of PtdE in acute cell death, the goal of this study was to develop and evaluate $^{99m}$Tc-duramycin as a novel molecular probe for imaging PtdE. **Methods:** Duramycin is covalently modified with succinimidyl 6-hydrazinonicotinate acetone hydrazone (HYNIC) and labeled with $^{99m}$Tc using a coordination chemistry involving tricine-phosphine coligands. The retention of PtdE-binding activities was confirmed using competition assays with PtdE-containing liposomes. The blood clearance, pharmacokinetics, and biodistribution of $^{99m}$Tc-duramycin were measured in rats. Finally, $^{99m}$Tc-duramycin binding to acute cell death in vivo was demonstrated using a rat model of acute myocardial infarction induced by ischemia and reperfusion and confirmed using autoradiography and histology. **Results:** HYNIC-derivatized duramycin with 1:1 stoicheometry was synthesized and confirmed by mass spectrometry. The radiolabeling efficiency was 80%–85%, radiochemical purity was 78%–89%, and specific activity was 54 GBq. The radiotracer was purified with high-performance liquid chromatography radiodetection before use. The specific uptake of $^{99m}$Tc-duramycin in apoptotic cells, compared with that in viable control cells, was enhanced by more than 30-fold. This binding was competitively diminished in the presence of PtdE-containing liposomes but not by liposomes consisting of other phospholipid species. Intravenously injected $^{99m}$Tc-duramycin has favorable pharmacokinetic and biodistribution profiles: it quickly clears from the circulation via the renal system, with a blood half-life of less than 4 min in rats. The hepatic and gastrointestinal uptake were very low. $^{99m}$Tc-duramycin is completely unmetabolized in vivo, and the intact agent is recovered from the urine. Combined with a fast clearance and low hepatic background, the avid binding of $^{99m}$Tc-duramycin to the infarcted myocardium quickly becomes conspicuous shortly after injection. The uptake of radioactivity in infarcted tissues was confirmed by autoradiography and histology. **Conclusion:** $^{99m}$Tc-duramycin is a stable, low-molecular-weight PtdE-binding radiopharmaceutical, with favorable in vivo imaging profiles. It is a strong candidate as a molecular probe for PtdE imaging and warrants further development and characterization.

**Key Words:** cardiology; molecular imaging; radiopharmaceuticals; $^{99m}$Tc; duramycin; γ-imaging

**J Nucl Med 2008; 49:1345–1352**
DOI: 10.2967/jnumed.107.048603

The noninvasive imaging of acute cell death, including apoptosis and necrosis, has important implications in the assessment of degenerative diseases and in the monitoring of tumor treatments. The drive to achieve better and earlier imaging necessitates a continual effort to explore novel uptake mechanisms and molecular probes that will lead to improved binding, pharmacokinetic, and biodistribution properties.

As a novel molecular target for apoptosis imaging, phosphatidylethanolamine (PtdE) is the second most abundant phospholipid and accounts for approximately 20% of all phospholipids in mammalian cellular membranes (*1,2*). Like phosphatidylserine (PtdS), PtdE is a constituent of the inner leaflet of the plasma membrane, with little presence on the surface of normal viable cells (*3*). In apoptosis, PtdE is exposed onto the cell surface as the redistribution of phospholipids across the bilayer is facilitated (*4*). In necrosis, PtdE becomes accessible to the extracellular milieu because of compromised plasma membrane integrity.

In contrast to PtdS, which when externalized serves as a signaling mechanism for the scavenging of the dying cells, the presence of PtdE on the apoptotic cell surface appears to play a regulatory role. Blebbing and the formation of apoptotic bodies are essential processes in which intracellular components are discretely packaged and designated for engulfment by scavenger cells without causing inflammation. As one of the morphologic hallmarks of apoptosis, blebbing is the consequence of profound membrane structural remodeling. The transbilayer movement of PtdE is especially

Received Oct. 24, 2007; revision accepted Apr. 11, 2008.
For correspondence or reprints contact: Ming Zhao, Department of Biophysics, Medical College of Wisconsin, 8701 Watertown Plank Rd., Milwaukee, WI, 53226.
E-mail: mzhao@mcw.edu

enhanced on the blebs of apoptotic cells (*5,6*). These morphologic changes are in part attributed to the PtdE-mediated reorganization of actin filaments (*5,6*).

As a potential molecular probe candidate for PtdE, duramycin is a 19–amino acid peptide produced by *Streptoverticillium cinnamoneus* (*7,8*). Duramycin binds the head group of PtdE with high affinity at a molar ratio of 1:1 (*9–11*). The overall structure of duramycin assumes a compact cyclic configuration, with a single binding pocket that specifically interacts with PtdE (*7,8*). Stabilized by 3 internal thioether linkages, duramycin is the smallest known polypeptide that has a defined 3-dimensional binding site (*7,8*). The binding pocket of duramycin resembles a glove-shaped surface that fits around the PtdE head group with well-defined physicochemical interactions. The hydrophobic binding pocket contains lipophilic side chains from Gly8, Pro9, and Val13. The binding of the ethanolamine head group is stabilized by an ionic interaction pair between the ammonium group of PtdE and the carboxylate of Asp15. This overall tight fit between the duramycin-binding pocket and the ethanolamine head group confers thermodynamic stability and an exclusive specificity for PtdE. In addition, 2 Phe side chains protrude from the upper loop, stabilizing the duramycin membrane binding by anchoring to the hydrophobic core of the membrane bilayer.

The biologic activities of duramycin and its close analog, cinnamycin, have been well characterized, and their PtdE-binding activity was used for in vitro biologic studies (*12–16*). Duramycin and cinnamycin have similar PtdE-binding activities, in which the 2 peptides differ by a single amino acid at the distal end away from the binding pocket. These peptides bind PtdE at an equal molar ratio with a dissociation constant in the nanomolar range (*14–16*). When fluorescently labeled, cinnamycin has been shown to bind to the externalized PtdE of apoptotic cells (*4*). Given the low molecular weight (MW), high stability, high binding affinity, and specificity, these peptides are potential candidates to be developed into molecular probes for in vivo applications.

The primary goal of this study was to synthesize and characterize $^{99m}$Tc-labeled duramycin for the noninvasive imaging of PtdE. In this article, we report the succinimidyl 6-hydrazinonicotinate acetone hydrazone (HYNIC) modification of duramycin and the radiolabeling and characterization of $^{99m}$Tc-duramycin as a PtdE-specific, fast-clearing molecular probe. The prompt and conspicuous imaging of acute cell death was demonstrated using an in vivo rat model of myocardial ischemia and reperfusion.

## MATERIALS AND METHODS

### High-Performance Liquid Chromatography (HPLC) Method 1

A $C_{18}$ column (pore size, 90 Å; 250 × 4.6 mm) (Jupiter; Phenomenex) was used with a mobile phase system consisting of acetonitrile and water at a flow rate of 1.0 mL/min at room temperature. A baseline of 5 min at 90% of buffer A (water with 0.1% trifluoroacetic acid, v/v) and 10% of buffer B (acetonitrile with 0.1% trifluoroacetic acid, v/v) was followed by a linear gradient to 10% of buffer A and 90% of buffer B in 35 min.

### HPLC Method 2

A Jupiter $C_{18}$ column (pore size, 90 Å; 250 × 4.6 mm) was used with a buffered mobile phase system consisting of a phosphate buffer (10 μM of sodium phosphate, pH 6.7) and acetonitrile at a flow rate of 1.0 mL/min at room temperature. A baseline of 5 min at 90% of buffer A (phosphate buffer, pH 6.7) and 10% of buffer B (acetonitrile) was followed by a linear gradient to 10% of buffer A and 90% of buffer B in 30 min. The level of radioactivity in the HPLC eluate was monitored by γ-counting at an energy window of 140 ± 15 keV.

### Radiolabeling of Duramycin

Duramycin was labeled with $^{99m}$Tc after HYNIC modification. Specifically, the HYNIC-conjugated duramycin was synthesized by reacting HYNIC with duramycin at a molar ratio of 8:1, in the presence of 4 equivalents of triethylamine. The reaction was performed in dimethylformamide for 18 h at room temperature with gentle stirring. HYNIC-conjugated duramycin was purified using HPLC method 1. The fractions that contained HYNIC-conjugated duramycin were pooled, aliquoted into 15-μg fractions, freeze-dried, and stored under argon at −80°C until use. The MW of the final product was confirmed using matrix-assisted laser desorption/ionization mass spectrometry. To synthesize a control peptide, which does not bind PtdE but has a minimally altered structure and the MW of duramycin, we inactivated duramycin by modifying a carboxylate group of Asp15 in the binding pocket. The blocking reaction was performed in dimethylformamide at room temperature, with duramycin, ethanolamine, and *N*-(3-dimethylaminopropyl)-*N*-ethylcarbodiimide hydrochloride at a molar ratio of 1:10:40. The inactivated compound, duramycin$^{I}$, was purified by $C_{18}$ reversed-phase HPLC. For radiolabeling, duramycin$^{I}$ was derivatized with HYNIC, purified by $C_{18}$ reversed-phase HPLC, and aliquoted as described earlier.

HYNIC-conjugated duramycin was labeled with $^{99m}$Tc using the tricine–phosphine coligand system. Specifically, 15 μg of HYNIC-conjugated duramycin was mixed with 40 mg of tricine, 1 mg of trisodium triphenylphosphine-3,3′,3″-trisulfonate (TPPTS), and 20 μg of $SnCl_2$ in 0.8 mL at pH 5.3. The labeling was initiated with the addition of about 37 MBq of $^{99m}$Tc. The incubation was allowed to proceed for 40 min at room temperature. The final radiopharmaceutical, $^{99m}$Tc-duramycin, was analyzed and purified using HPLC method 2. After purification, acetonitrile was removed by evaporation under nitrogen, and $^{99m}$Tc-duramycin was reconstituted in saline for use. $^{99m}$Tc-labeled duramycin$^{I}$ was synthesized in the same fashion. For stability tests, cysteine challenge was performed at a cysteine–to–$^{99m}$Tc-duramycin ratio of 100:1, in 0.01 μM of phosphate buffer (pH 6.8) for 2 h at room temperature. The sample was analyzed with HPLC radiodetection (radio-HPLC) (method 2).

### Preparation of Liposomes

Liposomes with the following chemical compositions were made: phosphatidylcholine (PtdC) (100%), PtdC/PtdE (50/50, w/w), PtdC/PtdS (50/50, w/w), and PtdC/phosphatidylglycerol (PtdG) (50/50, w/w). Solid phospholipids were weighed (2 mg) for each type of lipid in separate glass test tubes (10 × 140 mm). One milliliter of chloroform was used to completely dissolve the

phospholipid in each tube. The chloroform was evaporated under a stream of nitrogen, and the dried phospholipids formed a thin film of residue on the test tube wall. The samples were thoroughly dried under vacuum overnight. The next morning, each sample was resuspended in 2 mL of *N*-(2-hydroxyethyl)piperazine-*N*′-(2-ethanesulfonic acid) (HEPES) buffer (15 μM of HEPES, 120 μM of sodium chloride; pH 7.4) at 45°C. Each suspension was sonicated for 2–5 min at 15 s/cycle until the mixture turned opaque, which indicated the formation of multilaminar liposomes. The samples were kept on ice until use.

### In Vitro Binding Tests

The PtdE-binding activity of $^{99m}$Tc-duramycin was examined using binding assays in vitro. A good source of exposed PtdE was apoptotic Jurkat lymphocytes after incubation with a final concentration of camptothecin of 5 μM at 37°C in a humidified atmosphere, with 5% of $CO_2$. Nontreated control or treated cells were harvested by centrifugation at 800*g* for 5 min and resuspended at $2 \times 10^6$/mL. Radiolabeled duramycin or duramycin$^I$ was added to each milliliter of cells at a final concentration of 100 nM, and the binding was allowed to proceed for 5 min at room temperature. The mixture was then loaded onto a layer of Histopaque (Sigma-Aldrich Co.). After centrifugation at 800*g* for 5 min, the cell pellet was collected at the bottom of the tube below the Histopaque layer (the medium that contained the nonbound radioactivity remained above the Histopaque). The aqueous supernatant was removed by gentle aspiration. The tip of the tube that contained the pellet was cut off using a hot scalpel. Bound radioactivity was determined by direct γ-counting at an energy window of 140 ± 15 keV.

### Competition Assay

The retention of the binding activity was determined using a competition assay in the presence of PtdE-containing liposomes. PtdC/PtdE liposomes were prepared as described earlier. A binding assay was performed in triplicate, in the presence of increasing amounts of PtdC/PtdE liposomes, from 1 to 10 μM of final concentration, in 4-fold increments. The radioactivity bound to the cell pellet was determined by γ-counting as described earlier. The assay was repeated using liposomes containing other species of closely related phospholipids, including PtdC, PtdG, and PtdS.

### Blood Half-Life and Pharmacokinetic Studies

The animal protocol was approved by the Institutional Animal Care and Use Committee under the National Institutes of Health guidelines. Healthy Sprague–Dawley rats were injected with radiolabeled duramycin (2.3 nmol) via the tail vein. At 0, 1, 5, 15, 30, and 60 min, 50 μL of blood were withdrawn from a preinstalled femoral artery catheter and collected in heparinized tubes. The blood sample was centrifuged at 5,000*g*, and the radioactivity in the cellular and plasma fractions was measured separately by direct γ-counting using an energy window of 140 ± 15 keV. The data output included total blood activity with time and the activity associated with blood cells and the plasma, respectively. The blood half-life was measured in triplicate. To investigate the pharmacokinetics of the radiopharmaceutical, 10 μL of the plasma or urine sample were analyzed using HPLC method 2.

### Biodistribution Studies

Healthy Sprague–Dawley rats were injected with radiolabeled duramycin (2.3 nmol). A dynamic whole-body biodistribution profile was acquired using an in-house γ-camera (XRT; GE Healthcare). The anesthetized animal was continually imaged at an energy window of 140 ± 15 keV; field of view, 22.5 × 22.5 cm; and matrix, 128 × 128, at 1 min per image for up to 60 min after injection.

For quantitative biodistribution at each designated time point after intravenous injection of radiolabeled duramycin, a group of 4 rats was sacrificed. Various tissues were dissected, rinsed in saline, and weighed, and the level of radioactivity was determined using direct γ-counting (140 ± 15 keV).

### In Vivo Imaging of Acute Cardiac Cell Death Using a Rat Model of Ischemia and Reperfusion

Sprague–Dawley rats were intraperitoneally anesthetized with sodium pentobarbital (50 mg/kg of body weight). After tracheotomy and intubation, respiration was maintained using a rodent ventilator. The proximal left anterior descending coronary artery (LAD) was occluded using a 6.0 suture at 1 mm below the left atrial appendage. For the sham operation, the suture was passed underneath the LAD without ligation. The presence of acute ischemia or reperfusion was confirmed by paleness in the area at risk and changes in electrocardiogram profiles including immediate elevation of ST segment and significant increase in the QRS complex amplitude and width. The coronary ligation was continued for 30 min. After reperfusion, the chest wall was closed by suturing in layers, and ventilation was maintained until the rat could regain spontaneous respiration.

After 2 h of reperfusion, $^{99m}$Tc-duramycin or $^{99m}$Tc-duramycin$^I$ (2.3 nmol, ~7.4 MBq) was injected via the tail vein. Dynamic in vivo planar imaging was performed using a γ-camera (energy window, 140 ± 15 keV; matrix size, 128 × 128; field of view, 22.5 × 22.5 cm) at 5 min/image for 60 min. A static image with 500 K counts was acquired after dynamic imaging.

At the end of the imaging study, the animal was sacrificed. The heart was excised and quickly rinsed in saline. About 2 mL of 0.5% triphenyl tetrazolium chloride in a HEPES buffer (w/v) was infused retrograde into the aorta to stain the entire myocardium. After 15 min of incubation at 37°C, the heart was fixed in 4% formaldehyde. Short-axis sections of the heart with a thickness of about 500 μm were cut and exposed to film (BMX MS; Kodak) overnight at −80°C. After the film was developed, each corresponding slice was differentiated overnight in 1% of formaldehyde in phosphate-buffered saline (v/v). Digitized autoradiography and histology section images were visually inspected. For measuring the radioactivity uptake in the infarcted tissues, the heart was harvested and stained by triphenyl tetrazolium chloride as described earlier. Infarcted myocardium was dissected from the viable tissue. After weighing, the radioactivity in the specimen was measured by γ-counting with an energy window at 140 ± 15 keV. The data were converted to percentage injected dose per gram (%ID/g).

## RESULTS

### Bioconjugation and Radiolabeling

After conjugation, the MW of HYNIC-conjugated duramycin was confirmed using mass spectrometry (both expected and actual MW, 2,188.4 g/mol). At this MW, 1 HYNIC covalently attaches to each molecule of duramycin. The primary sequence of duramycin has 19 amino acids

in the order of CKQSCSFGPFTFVCDGNTK (Fig. 1A). Two primary amines are available for conjugation at the *N*-terminal and the side chain of Lys2 (Fig. 1A). It is likely that HYNIC-conjugated duramycin is in a form of isomers, where the HYNIC moiety is present on either Cys1 or Lys2. The duramycin conjugate with 2 HYNIC moieties was removed by HPLC purification and confirmed by mass spectrometry. Figure 1B demonstrates a typical radiochromatogram, in which $^{99m}$Tc-duramycin was eluted with a retention time of 24 min. At the current labeling condition, the labeling efficiency was 80%–85%, the radiochemical purity was between 78% and 89% before HPLC purification, and the specific activity was 54 GBq. Although column chromatography purification (Figs. 1B and 1C) is necessary to obtain the final radiopharmaceutical for further experiments, the current radiolabeling protocol is sufficiently amenable to conduct our preliminary studies. Once purified, $^{99m}$Tc-duramycin is stable, and no significant levels of detached $^{99m}$Tc were detected for at least 24 h in aqueous solution. This result is consistent with the prior report that a phosphine coligand substantially improves the stability of $^{99m}$Tc coordination, compared with tricine alone (*17,18*).

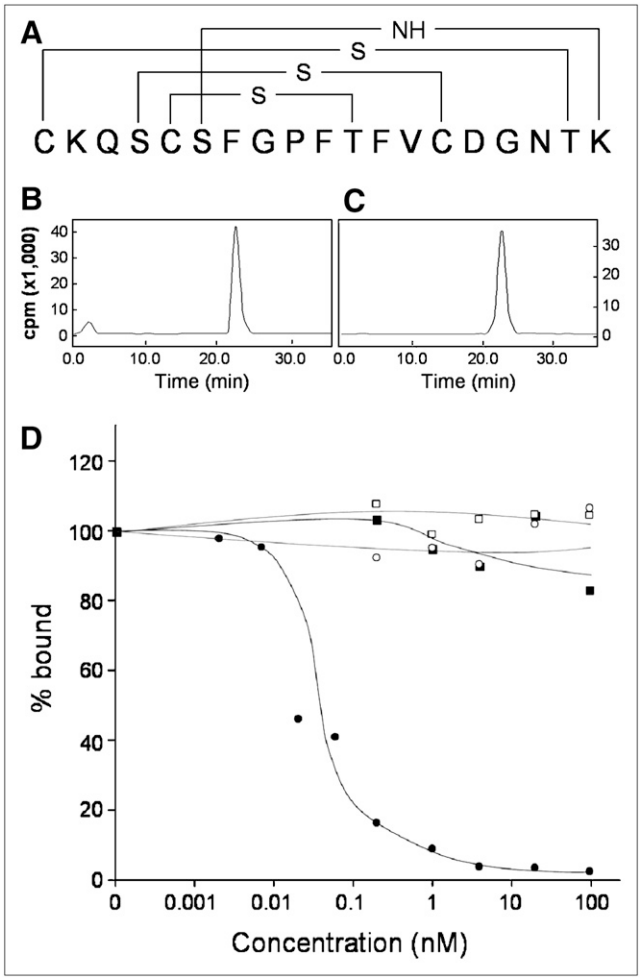


**FIGURE 1.** (A) Diagram illustrating primary structure of duramycin with cross-linking bridges. (B and C) Radio-HPLC chromatograms of $^{99m}$Tc-duramycin before and after purification are shown in B and C, respectively. Low, but significant, level of $^{99m}$Tc-pertechnetate is present before purification with retention time of 2 min. (D) Representative competition curve of 3 independent experiments. $^{99m}$Tc-duramycin binding of apoptotic cells is competitively diminished by presence of PtdE-containing liposomes (●) but not other phospholipid species, including PtdC (■), PtdG (□), or PtdS (○). cpm = counts per minute.

When the native form of duramycin was labeled with $^{99m}$Tc without HYNIC, the radiochemical yield was about 10%. In a cysteine challenge experiment, the radioactivity associated with the native duramycin was diminished by another 90% at a cysteine-to-duramycin ratio of 100:1. In contrast, under the same condition the radioactivity bound to HYNIC-conjugated duramycin was reduced by less than 3%. The native form of duramycin can indeed take up a limited amount of $^{99m}$Tc but does so only loosely, without, perhaps, forming a well-defined coordination complex. The presence of HYNIC, or another form of chelation core, is essential for the stable labeling of duramycin with $^{99m}$Tc.

### In Vitro Binding Tests

The cellular binding of $^{99m}$Tc-duramycin was dramatically enhanced in apoptotic versus viable control cells, and the binding was competitively abolished in the presence of PtdE-containing liposomes.

Specifically, $^{99m}$Tc-duramycin was incubated with $2 \times 10^6$ viable Jurkat lymphocytes as control or apoptotic cells induced by camptothecin treatment. Although the radioactivity uptake in viable cells remained near background, the binding of $^{99m}$Tc-duramycin to apoptotic cells was elevated by a factor of $32 \pm 6$ ($n = 3$). According to Figure 1D, this binding to the apoptotic cells was exclusively and competitively diminished in the presence of increasing concentrations of PtdE-containing liposomes. However, liposomes consisting of PtdC, PtdG, or PtdS were unable to competitively reduce the radioactivity uptake of $^{99m}$Tc-duramycin in apoptotic cells. $^{99m}$Tc-duramycin$^{I}$ bound to apoptotic cells at background levels only, and this binding was not competitively diminished in the presence of PtdE-containing liposomes (data not shown).

### Pharmacokinetics and Biodistribution of $^{99m}$Tc-Duramycin in Rats

After intravenous injection, $^{99m}$Tc-duramycin exhibited rapid clearance, with a blood half-life of less than 4 min (Fig. 2A). Of the radioactivity in the blood, greater than 95% was associated with the plasma fraction at all time points, confirming that $^{99m}$Tc-duramycin has minimal interactions with normal blood cells. According to radio-HPLC analysis of plasma samples, the majority of the injected radioactivity remains as the parent $^{99m}$Tc-duramycin (Figs. 2C and 2D). A minor peak is present with a longer retention time (27 min), which appears to be in equilibrium with an unknown blood component (Figs. 2C and 2D). The chemical species of this minor peak was not excreted by the renal

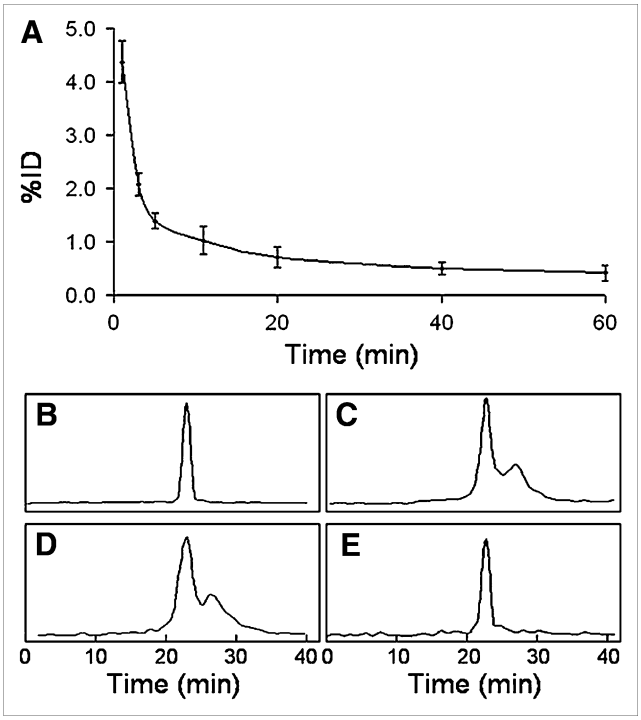


**FIGURE 2.** (A) Blood clearance of $^{99m}$Tc-duramycin in healthy rats ($n$ = 3). (B–E) Radio-HPLC chromatograms of $^{99m}$Tc-duramycin standard (B), serum at 1 min after injection (C), serum at 5 min after injection (D), and urine at 60 min after injection (E).

function because it was not detected in the urine. Radio-HPLC analysis of $^{99m}$Tc-duramycin in the presence of rat serum albumin did not result in any complex formation between the tracer and albumin. It is likely that after intravenous injection, $^{99m}$Tc-duramycin is associated to a degree with the lipoproteins, which are known to contain PtdE. The intravenously injected $^{99m}$Tc-duramycin showed no sign of metabolic degradation and was recovered intact from urine samples, in which neither additional radioactive derivatives nor $^{99m}$Tc-pertechnetate was detected (Fig. 2E).

For biodistribution, $^{99m}$Tc-duramycin renal excretion is the predominant route of clearance, with a low uptake in the hepatic and gastrointestinal regions (Table 1). The agent does not seem to cross the blood–brain barrier, because the brain uptake was low (Table 1). The presence of radioactivity in the lungs and the normal myocardium promptly approached background levels with time because of a rapid blood clearance, thus paving the way for an early and clear detection of acute cardiac cell death. This biodistribution profile was confirmed by in vivo dynamic studies using dynamic anterior planar scintigraphic imaging (Fig. 3A). At the current dosage tested, no signs of toxicity or other adverse effects were observed.

### In Vivo Imaging of Acute Cardiac Cell Death

In dynamic images, a focal uptake was seen at the infarct as early as 10 min after injection (Fig. 3B). The prompt

**TABLE 1**
Biodistribution of Intravenously Injected $^{99m}$Tc-Duramycin in Healthy Rats ($n$ = 4)

| Organ/tissue | Uptake (%ID/g) at 60 min after injection |
|---|---|
| Brain | 0.01 ± 0.01 |
| Thyroid | 0.08 ± 0.03 |
| Lung | 0.12 ± 0.05 |
| Heart | 0.21 ± 0.16 |
| Liver | 0.28 ± 0.01 |
| Pancreas | 0.05 ± 0.01 |
| Spleen | 0.10 ± 0.02 |
| Kidney | 2.32 ± 0.48 |
| Stomach | 0.11 ± 0.01 |
| Small intestine | 0.37 ± 0.07 |
| Colon | 0.11 ± 0.01 |
| Bone | 0.04 ± 0.01 |
| Muscle | 0.03 ± 0.01 |
| Fat | 0.06 ± 0.06 |
| Skin | 0.01 ± 0.01 |
| Blood | 0.33 ± 0.11 |
| Thymus | 0.06 ± 0.02 |
| Urine | 22.1 ± 13.25 |

blood clearance and low hepatic uptake facilitated an early and conspicuous appearance of the infarct. At 2 h after injection, the infarct-to-lung ratio was 4.8 ± 0.4 ($n$ = 3) and the infarct-to-muscle ratio was 12.2 ± 1.3 ($n$ = 3). The distribution of radioactivity in the autoradiography colocalized with the infarct in the histology of the myocardium (Fig. 3C, inset). The level of radioactivity remained persistent, with no washout over time. In contrast, the presence of $^{99m}$Tc-duramycin$^{I}$ in the infarcted heart was accompanied by a washout, a result consistent with the compromised PtdE-binding activity. At 1 h after injection, the average radioactivity at the infarct site was above 4.0 %ID/g for $^{99m}$Tc-duramycin, whereas that for $^{99m}$Tc-duramycin$^{I}$ was less than 1.0 %ID/g.

## DISCUSSION

The goal of the current study was to synthesize and characterize $^{99m}$Tc-duramycin as a potential molecular probe candidate for the noninvasive imaging of PtdE.

The in vivo stability of $^{99m}$Tc-duramycin can be attributed to at least the following 2 aspects. First, to preserve the convenience of HYNIC radiochemistry we adopted a phosphine compound as a third coligand, as described by Edwards et al. (*17,18*). To this end, although tricine alone has been widely used as a coligand for HYNIC radiochemistry, in which 2 tricine molecules form a well-defined coordination complex with $^{99m}$Tc and the hydrazine group of HYNIC, the tricine chelation core is known to be less stable under dilute conditions (*17–22*). By including TPPTS in the coordination chemistry, $^{99m}$Tc-duramycin remains stable both in solution and in vivo, consistent with the prior findings (*17,18*). The second key factor that contributes to the stability of $^{99m}$Tc-duramycin stems from

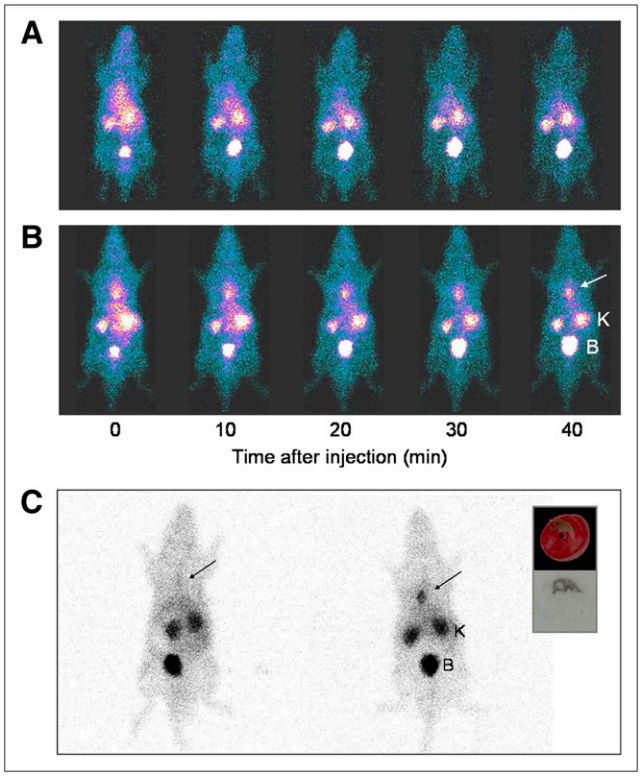


**FIGURE 3.** (A) Dynamic planar imaging of $^{99m}$Tc-duramycin distribution in healthy rat. Note rapid renal clearance of radiotracer and low hepatic uptake. (B) Whole-body dynamic planar imaging of $^{99m}$Tc-duramycin uptake in rat with acute myocardial infarction. (C) Non–color-enhanced, raw counts of static planar images of sham-operated rat (left) and infarcted rat (right) acquired at 120 min after intravenous injection of $^{99m}$Tc-duramycin. Infarct site is marked by arrows. In autoradiography, radioactivity uptake in myocardium colocalizes with infarct with excellent infarct-to-noninfarct ratio (inset). B = bladder; K = kidney.

the structural configuration of duramycin, in which the polypeptide is stabilized by 3 internal thioether bridges (*7,8*). In addition, the absence of a free peptidergic terminus as a result of the circularization of the polypeptide minimizes the chance of proteolytic degradation by blood-borne proteases and peptidases (*7,8*). The combination of a stable radiochemistry and the resistance to proteolytic or metabolic degradation synergistically contributes to the overall stability of $^{99m}$Tc-duramycin in solution and in vivo. These features were reflected in the absence of physicochemical degradation of $^{99m}$Tc-duramycin after intravenous injection and the recovery of the intact radiopharmaceutical in the urine samples.

According to the existing literature, the binding affinity of duramycin with PtdE-containing membranes is between 4.8 and 25.0 hM at concentrations that are relevant to an injection dosage for imaging (*10*). As the site of HYNIC attachment and radiolabeling is at the distal end of duramycin, away from the PtdE binding site, it is expected that the process of radiolabeling should have minimal interference with the interactions between duramycin and PtdE.

The avid accumulation of $^{99m}$Tc-duramycin in the region of infarction is presumably because of high levels of accessible PtdE as a result of extensive cell death, including apoptosis and necrosis. Although the exact roles and percentages of each mode of cell death after ischemia and reperfusion remain controversial, the uptake of $^{99m}$Tc-duramycin in the infarcted myocardium is likely to reflect an overall degree of cellular injuries, in which PtdE is available for binding in apoptotic cells because of externalization and in necrotic cells when the integrity of the plasma membrane is compromised (*23,24*). The early and prominent appearance of the hot-spot uptake at the infarct region also benefits from the prompt receding background due to a fast blood clearance. In addition, this conspicuous infarct detection is attributed to the low uptake in the hepatic area, which is near the heart. Although vascular hyperpermeability is a well-known consequence of acute myocardial infarction, no washout after the uptake suggests that passive uptake plays only a minor, if not negligible, role in $^{99m}$Tc-duramycin binding to the infarcted tissue. The PtdE-dependent uptake of $^{99m}$Tc-duramycin is evident from the lack of retention in the infarct tissue when duramycin is inactivated, as in the case of $^{99m}$Tc-duramycin$^{I}$. This conclusion is supported by the washout of other nonspecific contrast agents from infarct tissues in prior imaging and histology studies by the authors of the current article and others (*25–27*).

Phospholipid-binding molecular probes hold promise in the noninvasive detection and quantification of acute cell death, taking advantage of the asymmetric distribution of defined phospholipid species between the plasma membrane bilayer. Among these, the characterization and utilities of annexin V and the C2A domain of synaptotagmin I have been reported in various applications (*27–41*). Both annexin V and C2A are calcium-dependent phospholipid-binding proteins, in which calcium ions in the binding pocket mediate the binding between the protein and the lipid membrane in the form of calcium bridges (*42,43*). In comparison, the binding between duramycin and PtdE is calcium-independent, involving multiple interactions of the peptide side chains with the ethanolamine head group and the hydrophobic fatty acid tails (*7,8*). Another striking feature of duramycin is its low molecular weight. At 2 kDa, duramycin is substantially smaller than annexin V (32–36 kDa) and C2A (12 kDa). The drastically enhanced rate of blood clearance of $^{99m}$Tc-duramycin is consistent with its low molecular weight and is apparent from the collection of bulk of the injected dose in the urine.

Although it is possible that PtdE binding may be accompanied by nonspecific uptake, we found no evidence of such a case. According to our biodistribution study, the uptake of $^{99m}$Tc-duramycin was generally low in tissues, including the liver. This finding was consistent with the results of in vivo whole-body imaging, in which $^{99m}$Tc-duramycin was cleared via the renal–urinary system without significant retention in the body. In future studies, we

will continue to characterize the tissue uptake of $^{99m}$Tc-duramycin and look for signs of nonspecific binding.

Duramycin is produced by *Streptoverticillium cinnamoneus,* in which immunogenicity may become a concern. However, duramycin is an antibiotic used to treat certain types of bacterial infections, including in patients with cystic fibrosis. The lack of significant toxicity and immunogenicity is evident from clinical practice involving duramycin. Although it is beyond the scope of the current article, the investigation of the immune response of duramycin and its derivatives will be an important aspect in future studies.

Some limitations of the current study include the following. First, HPLC purification is necessary to obtain the radiotracer at satisfactory radiochemical quality for in vivo imaging. This shortcoming will be overcome by optimizing radiolabeling conditions toward a single-step labeling protocol without further purification needed. Second, the HYNIC-derivatized duramycin, and therefore the radiolabeled compound, are not isomerically homogeneous, because 2 primary amines are on the surface of duramycin. This issue will be resolved in future studies by point mutations that eliminate 1 of the amines.

$^{99m}$Tc-labeled duramycin using the HYNIC-tricine-phosphine chelation core is highly stable in solution and in vivo. The PtdE-binding activity and specificity of $^{99m}$Tc-duramycin are well preserved after radiolabeling. The radiopharmaceutical has favorable pharmacokinetic and biodistribution profiles in vivo. Combined with a fast blood clearance and low hepatic uptake, an avid binding of $^{99m}$Tc-duramycin to the site of acute myocardial infarction allows prompt and conspicuous imaging shortly after injection. This novel agent is a promising molecular probe for the noninvasive imaging of PtdE with clinical implications and warrants further development and characterization.

## ACKNOWLEDGMENTS

The authors are grateful to Carrie M. O'Connor for editorial help. This work was supported in part by the American Heart Association grant 0435147N.

## REFERENCES

1. Alberts B, Johnson A, Lewis J, et al. *Molecular Biology of the Cell.* 4th ed. New York, NY: Garland Science; 2002.
2. Spector AA, Yorek MA. Membrane lipid composition and cellular function. *J Lipid Res.* 1985;26:1015–1035.
3. Bevers EM, Comfurius P, Dekkers DW, et al. Lipid translocation across the plasma membrane of mammalian cells. *Biochim Biophys Acta.* 1999;1439:317–330.
4. Emoto K, Toyama-Sorimachi N, Karasuyama H, et al. Exposure of phosphatidylethanolamine on the surface of apoptotic cells. *Exp Cell Res.* 1997;232:430–434.
5. Umeda M, Emoto K. Membrane phospholipid dynamics during cytokinesis: regulation of actin filament assembly by redistribution of membrane surface phospholipid. *Chem Phys Lipids.* 1999;101:81–91.
6. Mills JC, Stone NL, Erhardt J, et al. Apoptotic membrane blebbing is regulated by myosin light chain phosphorylation. *J Cell Biol.* 1998;140:627–636.
7. Hayashi F, Nagashima K, Terui Y, et al. The structure of PA48009: the revised structure of duramycin. *J Antibiot (Tokyo).* 1990;43:1421–1430.
8. Zimmermann N, Freund S, Fredenhagen A, et al. Solution structures of the lantibiotics duramycin B and C. *Eur J Biochem.* 1993;216:419–428.
9. Marki F, Hanni E, Fredenhagen A, et al. Mode of action of the lanthionine-containing peptide antibiotics duramycin, duramycin B and C, and cinnamycin as indirect inhibitors of phospholipase A2. *Biochem Pharmacol.* 1991;42:2027–2035.
10. Iwamoto K, Hayakawa T, Murate M, et al. Curvature-dependent recognition of ethanolamine phospholipids by duramycin and cinnamycin. *Biophys J.* 2007;93:1608–1619.
11. Seelig J. Thermodynamics of lipid-peptide interactions. *Biochim Biophys Acta.* 2004;1666:40–50.
12. Aoki Y, Uenaka T, Aoki J, et al. A novel peptide probe for studying the transbilayer movement of phosphatidylethanolamine. *J Biochem (Tokyo).* 1994;116:291–297.
13. Machaidze G, Ziegler A, Seelig J. Specific binding of Ro 09-0198 (cinnamycin) to phosphatidylethanolamine: a thermodynamic analysis. *Biochemistry.* 2002;41:1965–1971.
14. Guder A, Wiedemann I, Sahl HG. Posttranslationally modified bacteriocins: the lantibiotics. *Biopolymers.* 2000;55:62–73.
15. Hosoda K, Ohya M, Kohno T, et al. Structure determination of an immunopotentiator peptide, cinnamycin, complexed with lysophosphatidylethanolamine by $^{1}$H-NMR1. *J Biochem (Tokyo).* 1996;119:226–230.
16. Kaletta C, Entian KD, Jung G. Prepeptide sequence of cinnamycin (Ro 09-0198): the first structural gene of a duramycin-type lantibiotic. *Eur J Biochem.* 1991;199:411–415.
17. Edwards DS, Liu S, Barrett JA, et al. New and versatile ternary ligand system for technetium radiopharmaceuticals: water soluble phosphines and tricine as coligands in labeling a hydrazinonicotinamide-modified cyclic glycoprotein IIb/IIIa receptor antagonist with $^{99m}$Tc. *Bioconjug Chem.* 1997;8:146–154.
18. Liu S, Edwards DS, Barrett JA. $^{99m}$Tc labeling of highly potent small peptides. *Bioconjug Chem.* 1997;8:621–636.
19. Liu S, Edwards DS, Looby RJ, et al. Labeling a hydrazino nicotinamide-modified cyclic IIb/IIIa receptor antagonist with $^{99m}$Tc using aminocarboxylates as coligands. *Bioconjug Chem.* 1996;7:63–71.
20. Babich JW, Solomon H, Pike MC, et al. Technetium-99m-labeled hydrazino nicotinamide derivatized chemotactic peptide analogs for imaging focal sites of bacterial infection. *J Nucl Med.* 1993;34:1964–1974.
21. Babich JW, Fischman AJ. Effect of "co-ligand" on the biodistribution of $^{99m}$Tc-labeled hydrazino nicotinic acid derivatized chemotactic peptides. *Nucl Med Biol.* 1995;22:25–30.
22. Liu S, Edwards DS, Looby RJ, et al. Labeling cyclic glycoprotein IIb/IIIa receptor antagonists with $^{99m}$Tc by the preformed chelate approach: effects of chelators on properties of [$^{99m}$Tc]chelator-peptide conjugates. *Bioconjug Chem.* 1996;7:196–202.
23. Kostin S, Pool L, Elsasser A, et al. Myocytes die by multiple mechanisms in failing human hearts. *Circ Res.* 2003;92:715–724.
24. Freude B, Masters TN, Kostin S, et al. Cardiomyocyte apoptosis in acute and chronic conditions. *Basic Res Cardiol.* 1998;93:85–89.
25. Kim RJ, Chen EL, Lima JAC, et al. Myocardial Gd-DTPA kinetics determine MRI contrast enhancement and reflect the extent and severity of myocardial injury after acute reperfused infarction. *Circulation.* 1996;94:3318–3326.
26. Zhu X, Zhang R, Campagna NF, et al. Assessment of reperfused myocardial infarction in the hyper-acute phase with delayed enhancement magnetic resonance imaging. *J Cardiovasc Magn Reson.* 2006;8:461–467.
27. Zhao M, Zhu X, Ji S, et al. $^{99m}$Tc-labeled C2A domain of synaptotagmin I as a target-specific molecular probe for noninvasive imaging of acute myocardial infarction. *J Nucl Med.* 2006;47:1367–1374.
28. Zhu X, Li Z, Zhao M. Imaging acute cardiac cell death: temporal and spatial distribution of $^{99m}$Tc-labeled C2A in the area at risk after myocardial ischemia and reperfusion. *J Nucl Med.* 2007;48:1031–1036.
29. Liu Z, Zhao M, Zhu X, et al. In vivo dynamic imaging of myocardial cell death using $^{99m}$Tc-labeled C2A domain of synaptotagmin I in a rat model of ischemia and reperfusion. *Nucl Med Biol.* 2007;34:907–915.
30. Audi S, Poellmann M, Zhu X, et al. Quantitative analysis of $^{99m}$Tc-C2A-GST distribution in the area at risk after myocardial ischemia and reperfusion using a compartmental model. *Nucl Med Biol.* 2007;34:897–905.
31. Zhao M, Beauregard DA, Loizou L, et al. Non-invasive detection of apoptosis using magnetic resonance imaging and a targeted contrast agent. *Nat Med.* 2001;7:1241–1244.
32. Fang W, Wang F, Ji S, et al. SPECT imaging of myocardial infarction using $^{99m}$Tc-labeled C2A domain of synaptotagmin I in a porcine-ischemia reperfusion model. *Nucl Med Biol.* 2007;34:917–923.
33. Jung HI, Kettunen MI, Davletov B, et al. Detection of apoptosis using the C2A domain of synaptotagmin I. *Bioconjug Chem.* 2004;15:983–987.
34. Krishnan AS, Neves AA, de Backer MM, et al. Detection of cell death in tumors by using MR imaging and a gadolinium-based targeted contrast agent. *Radiology.* 2008;246:854–862.

35. Tait JF, Smith C, Blankenberg FG. Structural requirements for in vivo detection of cell death with $^{99m}$Tc-annexin V. *J Nucl Med.* 2005;46:807–815.
36. Hofstra L, Liem IH, Dumont EA, et al. Visualisation of cell death in vivo in patients with acute myocardial infarction. *Lancet.* 2000;356:209–212.
37. Blankenberg FG, Katsikis PD, Tait JF, et al. In vivo detection and imaging of phosphatidylserine expression during programmed cell death. *Proc Natl Acad Sci USA.* 1998;95:6349–6354.
38. Ohtsuki K, Akashi K, Aoka Y, et al. Technetium-99m HYNIC-annexin V: a potential radiopharmaceutical for the in-vivo detection of apoptosis. *Eur J Nucl Med.* 1999;26:1251–1258.
39. Petrovsky A, Schellenberger E, Josephson L, et al. Near-infrared fluorescent imaging of tumor apoptosis. *Cancer Res.* 2003;63:1936–1942.
40. Lahorte CMM, VanderHeyden JL, Steinmetz N, et al. Apoptosis-detecting radioligands: current state of the art and future perspectives. *Eur J Nucl Med Mol Imaging.* 2004;31:887–919.
41. Sosnovik DE, Schellenberger EA, Nahrendorf M, et al. Magnetic resonance imaging of cardiomyocyte apoptosis with a novel magneto-optical nanoparticle. *Magn Reson Med.* 2005;54:718–724.
42. Huber R, Romisch J, Paques EP. The crystal and molecular structure of human annexin V, an anticoagulant protein that binds to calcium and membranes. *EMBO J.* 1990;9:3867–3874.
43. Sutton RB, Davletov BA, Berghuis AM, Sudhof TC, Sprang SR. Structure of the first C2 domain of synaptotagmin I: a novel Ca2+/phospholipid-binding fold. *Cell.* 1995;80:929–938.

The Journal of NUCLEAR MEDICINE

# $^{99m}$Tc-Labeled Duramycin as a Novel Phosphatidylethanolamine-Binding Molecular Probe

Ming Zhao, Zhixin Li and Scott Bugenhagen

*J Nucl Med.* 2008;49:1345-1352.
Published online: July 16, 2008.
Doi: 10.2967/jnumed.107.048603



*The Journal of Nuclear Medicine* is published monthly.
SNMMI | Society of Nuclear Medicine and Molecular Imaging
1850 Samuel Morse Drive, Reston, VA 20190.
(Print ISSN: 0161-5505, Online ISSN: 2159-662X)



SNMMI SOCIETY OF NUCLEAR MEDICINE AND MOLECULAR IMAGING